ELSEVIER

Contents lists available at ScienceDirect

Journal of Building Engineering

journal homepage: http://www.elsevier.com/locate/jobe





Thin slender concrete rectangular walls in moderate seismic regions with a single reinforcement layer

Carlos Blandón a,*, Ricardo Bonett b

- a Department of Civil Engineering, Universidad EIA, Envigado, Colombia
- ^b Department of Civil Engineering, Universidad de Medellín, Colombia

ARTICLE INFO

Keywords: Thin wall Slender wall Reinforced concrete Cyclic behavior Buckling Welded wire mesh

ABSTRACT

Some Latin-American countries, including Colombia, Peru, Panamá and the Dominican Republic, have adopted an industrialized system for the construction of buildings using thin slender reinforced concrete walls. The main advantage of this system is that it can increase the construction speed and reduce the use of nonstructural walls. as all architectonical spaces are defined by the structural walls. Additionally, designers tend to use thin structural walls with low steel reinforcement ratios, which is reflected in a reduction of the construction cost. The typical wall section for 6 to 10-story buildings is characterized by a thickness of around 100 mm and a single layer of welded wire mesh acting as longitudinal and transverse reinforcement. Additional reinforcing bars may be placed at the wall edges to increase moment capacity, but in most cases, there are no confined boundary elements along the edges. Despite the system's popularity, experimental data for these types of walls is still scarse. In addition to this, structural walls of low thickness and high aspect ratio with unconfined or poorly confined boundary elements have shown structural deficiencies in the 2010 Central Valley Chile earthquake. In this paper, existing and new experimental data from representative thin slender walls, used in moderate seismic regions, was analyzed to evaluate the structural system under lateral loads. Two unconfined reinforced concrete walls with typical section detailing were tested. Additionally, these tests were complemented with an experimental database of 28 rectangular wall units of thickness less than 100 mm, as reported in the literature. This data was used to analyze the behavior of rectangular thin slender walls in terms of axial load ratio, boundary elements conditions, plastic hinge length, and maximum drift capacity. The experimental data shows a significant reduction in drift capacity as axial load, clear interstory height to wall thickness ratio, or wall length increases. It is also evident that plasticity is concentrated at the base of the walls, mainly due to the low vertical reinforcement ratios. Finally, a capacity vs. demand stochastic analysis was carried out to evaluate the performance of buildings up to 10 stories in a moderate seismic zone. These analyses show that for moderate seismic regions the probability of reaching a severe damage limit state is low for buildings configured with rectangular walls having a single layer of reinforcement.

1. Introduction

Some Latin American countries have adopted a technique for the construction of reinforced concrete wall buildings that reduce construction time and costs based on the reduction of concrete volume, reinforcing steel and non-structural partitions. This technique has proven to be efficient from the construction point of view; therefore, the total height of buildings constructed using this method has been gradually increasing, exceeding more than 20 stories nowadays. The success of this construction method is mainly because structural walls are cast-

in-place conforming the structural system and the architectonical spaces simultaneously.

The structural design of these buildings follows current construction codes, which are based on the ACI standards. For instance, for the Colombian case, the current code (NSR-10) [1] is based mainly on the ACI 318–08 [2] version for reinforced concrete structures. The main problem identified with these buildings is that they have several characteristics that are significantly different from the traditional reinforced concrete walls buildings and there is limited information to define if the design procedure and equations defined in the codes may be directly

E-mail addresses: carlos.blandon@eia.edu.co (C. Blandón), rbonett@udem.edu.co (R. Bonett).

^{*} Corresponding author.

applied to elements and structures with such characteristics.

The main differences of the buildings constructed with the method previously described, compared to the traditional method are: thin walls with thickness between 80 mm to 150 mm (resulting in large out-ofplane slenderness ratios larger than 20), light steel ratios along the web of the wall (close to the minimum of 0.25%), low ductility welded wire mesh used as main reinforcement of the wall, large steel ratios at wall edges and unconfined wall edges [3,4]. Based on the damage observations from past earthquakes in Chile (2010) and New Zealand (2011), some of these characteristics were defined as possible reasons for the damage observed [5,6]. For instance, Alarcón et al. [7] mentioned that the brittle damage of walls during the earthquake in 2010 in Chile was due to poor confinement and lack of reinforcement bar restrain, associated to moderate and large axial load ratios. Kam et al. [8] also mention that the concrete strain capacity of thin walls without confinement could be less than typical values used for design. This is consistent with previous studies about the limited displacement capacity of wall with poor or absent confinement of the wall boundaries

Based on the fracture of the longitudinal reinforcement of some walls on modern buildings during the New Zealand earthquake, Kam et al. [8] discuss the necessity of evaluating the current code requirements for the minimum vertical steel reinforcement ratio. This is in accordance with Dazio et al. [10] who carried out cyclic testing of walls with different steel ratios and reported that the length where plastic deformations concentrate is reduced as the steel ratio decreases. The effect of using light reinforcement ratio along the web had been also previously reported by Dai [12] and Lefas and Kotsovos [13], which indicated that this practice results in enlarged cracks. Additionally, the problem presented in these references is consistent with the recent recommendations made by Lu et al. [14] to increase the minimum vertical steel ratio of ductile walls to ensure a proper plasticity distribution along the wall height. Regarding the large out-of-plane slenderness, Paulay and Priestley [15] discussed the effect of lateral instability in thin walls due to reversed loading cycles. These authors indicate that RC walls may present an out-of-plane displacement during the closure of the cracks formed due to the in-plane cyclic loading. Because the walls used as part of the structural system under study may have a thickness as low as 80 mm, it is likely that out-of-plane instability may occur during seismic loading. Rosso et al. [16] also reported that the use of a single layer of reinforcing steel might increase the out-of-plane instability problem. This behavior was also captured during an experimental program reported by Almeida [17] which included a 80 mm thick T-shape wall, reinforced with ductile bars, subjected to cyclic loading. The results of the experiment showed that the wall could only sustain a drift capacity below 0.7% due to a compressive failure of the web, buckling of the reinforcement and a significant out-of-plane response during the cycles.

Regarding the use of welded wire mesh, there are a few references that show the limited displacement capacity of walls reinforced with this type of steel [18,19], of shear controlled squat walls used for low rise constructions.

The existing studies indicate that as the walls thickness is reduced, the ductility capacity decreases [4,20]; however, none of these studies provides data about the behavior of flexure-controlled rectangular thin walls below 100 mm thickness with a single layer of low ductility welded wire mesh reinforcing steel. This document provides additional experimental information about this type of walls, from specimen with characteristics defined based on a building database gathered from a set of buildings located in a moderate seismic hazard area. These types of walls are frequently used for the construction of 6-to 12 story buildings in moderate seismic hazard areas. However, strong ground motions have not been recorded in these areas and therefore, the seismic behavior of these slender and thin walls have not been evaluated directly in the field. Additionally, existing experimental information of thin reinforced concrete walls, reported in other references, were also analyzed to define the performance of flexure-controlled rectangular thin walls under

lateral load.

2. Characteristics of surveyed thin slender concrete wall buildings

Structural drawings from 14 buildings between 6 and 12 stories constructed using the system previously described, located in a moderated seismicity region in Colombia, were analyzed to define the main characteristics of rectangular walls within these buildings. The buildings were built between 2007 and 2014. The gravity-load-resisting systems of the buildings correspond to flat plate floor systems, where a slab of uniform thickness spans between walls. The wall area in each direction, as a percentage of a total floor area, is between 1.3% and 4.6%. From the database, it was found that the thickness of the walls ranged between 80 mm to 150 mm with aspect ratios above 4.0 and in some cases exceeding a value of 20.0. The mean axial load ratio was 6.9% and the maximum recorded value was close to 18%. Walls with thickness below 120 mm are reinforced with only one layer of steel consisting on low ductility welded wire mesh. The vertical steel ratio along the wall ranges between 0.2% and 0.5%. This ratio may be larger at the edges of the wall were additional reinforcement bars may be concentrated. Table 1 shows the main characteristic of the buildings where B₁ and B_t correspond to long side and short side, D1 and Dt are the wall area in longitudinal and transversal direction as a percentage of the total floor area, T₁ and T_t are the fundamental period in each direction.

The most critical sections identified during the survey study are shown in Fig. 1. A common detail is to use only cold-drawn welded wire mesh as vertical and transverse reinforcement of the wall (Fig. 1a). In some cases, the mesh is embedded inside the foundation and into the wall; there are cases where instead of placing the mesh inside the foundation, which poses a constructive difficulty, conventional starter #2 (6 mm) or #3 (9 mm) reinforcement bars are cast inside the foundation. Once the foundations are completed, the mesh is spliced with the starter bars. It is also common to find additional conventional steel reinforcement bars at the wall ends anchored at the foundation, which complements the steel mesh placed along the center portion of the wall section (Fig. 1b). The additional reinforcement is placed at the end of the walls in one or two layer depending on the wall thickness. For walls with thickness greater than or equal to 120 mm, two layers of reinforcement are commonly used with or without boundary elements (Fig. 1(d), (e) and 1(f)). When stirrups or hooks are present, evaluated walls exhibit a confined core area for the boundary elements that represents a maximum of 30% of the transverse section, and the minimum space between layers can be around $10d_h$ (Fig. 1(c) and (f)). These details indicate that the confinement that can be effectively obtained in the core

Table 1Main characteristics of buildings from the database.

ID	Number of Stories	Height, Hw (m)	Bl (m)	Bt (m)	Wall area (as % of floor area)		Period	
					Dl (%)	Dt (%)	Tl (s)	Tt (s)
1	12	28.8	23.0	12.4	1.4	2.1	0.68	0.52
2	11	29.6	21.4	14.8	1.6	1.5	0.74	0.86
3	5	13.8	23.1	8.1	1.3	2.0	0.25	0.14
4	9	20.7	21.0	11.5	1.9	3.5	0.49	0.35
5	7	20.5	18.5	12.4	1.9	3.4	0.37	0.24
6	8	19.2	49.0	15.7	2.0	2.6	0.43	0.30
7	12	34.1	28.5	13.4	1.9	4.0	0.70	1.54
8	12	33.4	31.6	18.3	1.9	4.2	0.63	0.56
9	6	14.7	20.2	14.9	1.6	3.5	0.33	0.54
10	12	29.4	21.8	16.2	2.1	4.6	0.82	0.93
11	9	23.0	44.4	18.5	1.4	3.1	0.65	0.48
12	6	14.8	20.5	14.9	1.4	3.8	0.36	0.60
13	6	15.0	17.6	16.2	2.3	4.5	0.27	0.29
14	8	20.0	52.4	20.9	1.7	3.4	0.38	0.66

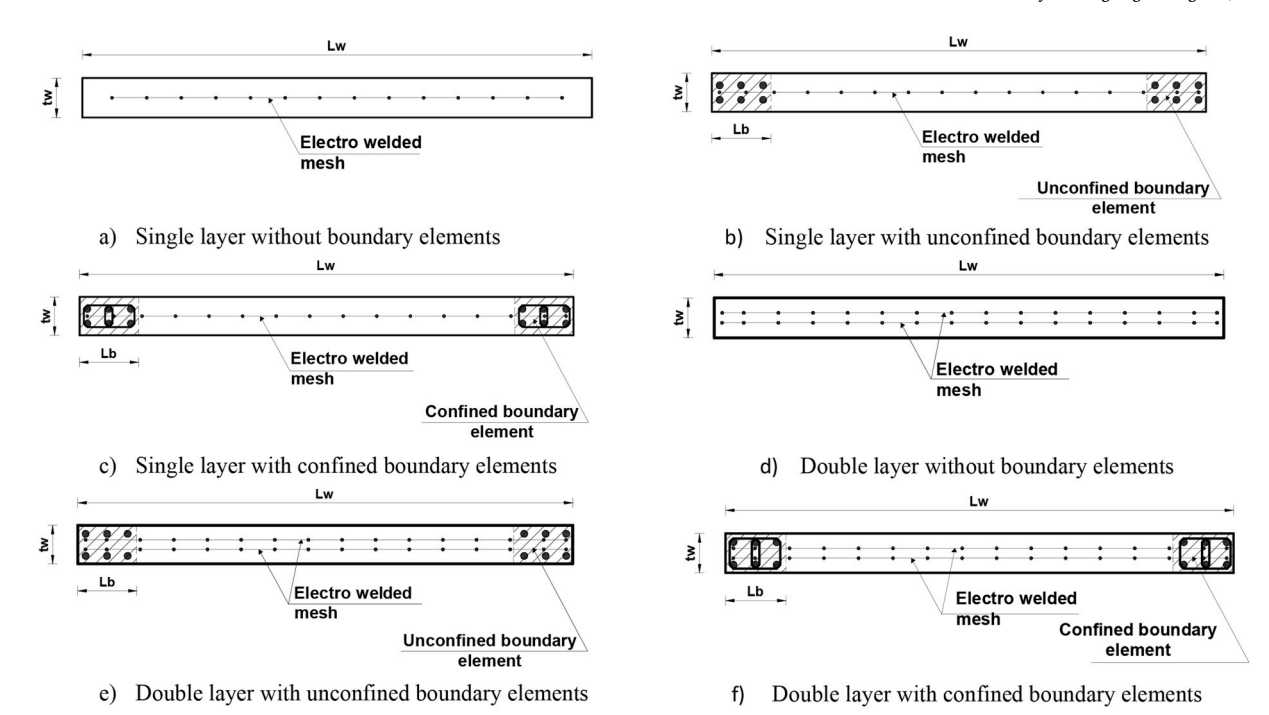


Fig. 1. Plans for some surveyed sections.

Table 2 Summary of database.

Author	Test	L_w (mm)	H_w (mm)	t_w (mm)	ρ (%)	f_c (MPa)	f_y^a (MPa)	ρ_h (%)	ALR	$M/VL_{w}(m)$	H_w/t_w	δ_f (%)	s/d_b
Oesterle et al. [21]	R1	1905	4560	102	0.5	45.3	519	0.31	N.A.	2.4	44.7	2.10	11.3
	R2	1905	4560 ^b	102	1.0	47.1	457	0.31	N.A.	2.4	10.8	2.67	2.8
Thomsen and Wallace [22]	RW1	1220	3810	102	1.0	31.6	434	0.33	0.1	3	37.5	1.90	8
	RW2	1220	3660	102	1.0	43.7	434	0.33	0.1	3	36.0	2.50	5.3
Su and Wong [23]	W1	400	1580	80	1.96	50.2	412	0.54	0.25	3.94	19.7	1.90	3.75–12.5 ^c
	W2	400	1580	80	1.96	41.8	412	0.54	0.5	3.94	19.7	1.20	
	W3	400	1580	80	1.96	42.9	412	1.08	0.5	3.94	19.7	1.10	
Alarcón et al. [24]	W1	700	1750	100	1.3	27.4	469.2	0.44	0.15	2.5	9	2.10	9^{d}
	W2	700	1750	100	1.3	27.4	469.2	0.44	0.25	2.5	9	1.80	
	W3	700	1750	100	1.3	27.4	469.2	0.44	0.35	2.5	9	1.50	
Hube et al. [20]	W4	700	1750	75	1.1	27.4	469.2	0.46	0.15	2.5	8	1.60	8^{d}
	W5	700	1330	100	1.3	27.4	469.2	0.44	0.15	1.9	9	1.80	9^d
	W6	700	1750	100	1.4	27.4	469.2	0.44	0.15	2.5	11	2.10	11.25 ^d
	W7	700	1750	100	1.3	27.4	469.2	0.44	0.15	2.5	9	2.40	9^{d}
	W8	700	1750	100	1.3	27.4	469.2	0.64	0.15	2.5	9	2.70	9 ^e
	W9	700	1750	100	1.3	27.4	469.2	0.56	0.15	2.5	9	2.70	9–11.25°
Pilakoutas and Elnashai [25]	SW4	600	1200	60	2.83	36.9	500	0.39	N.A	2.1	20	1.81	_
	SW6	600	1200	60	2.83	38.6	500	0.31	N.A	2.1	20	1.64	_
	SW7	600	1200	60	3.02	32.0	540	0.39	N.A	2.1	20	1.67	_
	SW8	600	1200	60	2.93	45.8	550	0.31	N.A	2.1	20	1.98	_
	SW9	600	1200	60	2.93	38.9	550	0.31	N.A	2.1	20	1.99	_
Goodsir [26]	W1	1500	3175	100	1.7	28.6	450	0.7	0.26	2.12	10	1.95	6
	W2	1500	3175	100	1.7	25.3	450	0.7	0.16	2.12	10	2.36	3.3
McMenamin [27]	4	1000	2500	50	0.6	60.6	504	0.4	N.A.	2.5	50	1.00	25
	5	1000	2500	50	1.1	37.1	504	0.4	N.A.	2.5	50	2.00	25
Chiewanichakorn [28]	1	1000	3750	50	1.26	39.3	318	0.15	0.002	3.75	75	0.90	7.5
	2	1000	3750	50	1.26	43.9	318	0.15	0.009	3.75	75	0.93	7.5
	3	1000	3750	50	1.26	23.0	318	0.19	0.004	3.75	75	1.17	6
	4	1000	3750	50	1.26	30.3	318	0.19	0.013	3.75	75	1.43	6
Almeida et al. [17]	TW1 ^f	2700	2000	80	0.67	28.8	565	0.15	0.043	3.7	25	0.70	12.5
	TW4 ^f	2700	2000	80	0.67	31.2	515	0.36	0.033	3.7	25	0.75	12.5

^a Strength for largest diameter reinforcement bar.

^b Height modified to 1.1 m during the test when the wall started to buckle.

^c Edge reinforcement - distributed reinforcement.

^d Edge bars only.

^e Boundary element bars only.

^f Single curtain steel reinforcement.

and the bar buckling restriction are limited.

3. Experimental database

Data from unidirectional in-plane tests of thin rectangular slender walls presenting flexural failure mode were gathered to evaluate the drift capacity of these type of walls and to establish the influence of different variables. Only specimen with thickness between 50 mm and 100 mm and overturning moment versus shear force ratios (*M/V*) larger than two were considered. Twenty-eight tests from nine different testing campaigns were found in the literature, most of them representing reduced scale walls (Table 2). Only eight of them had a single layer of reinforcement, and six of those represented precast walls with practically no axial load and had special connection details at the foundation-wall interface. Some of the main characteristics associated to the failure mode are discussed in Table 3.

4. Experimental test

The existing literature does not provide experimental information about rectangular thin reinforced concrete walls reinforced with low ductility steel mesh reinforcement and complementary reinforcement at the edges, which is a typical detail of the walls of interest, as previously shown in Figure 1. These type of walls are often used to resist the seismic demand in moderate seismic zones for 6 to 12 story buildings despite having high aspect ratios and no confined boundary elements. To complement the existing information, two full-scale $(1200 \text{ mm} \times 80 \text{ mm} \text{ walls [W1 and W2]})$ with a 2.4 m story height were carried out on specimens defined based on the set of buildings surveyed. The specimen was reinforced with a low ductile welded wire mesh with a transverse and longitudinal area of 158 mm²/m (5.5 mm bidirectional wires each 150 mm) and one additional 16 mm (#5) reinforcement bar located 60 mm from the end of the wall, conforming an unconfined edge element, as shown in Fig. 2. This reinforcement corresponds to a steel ratio of 0.20% in the center of the wall and 3.1% at the edge of the wall, considering an edge area of 80 mm, which is the wall thickness, by 120 mm, which is twice the distance from the edge of the wall to the reinforcement bar location. The 16 mm bars extended from the foundation to the top of the wall without lap splices while the mesh was spliced 600 mm from the wall-foundation interface with four additional 6 mm dowels anchored to the foundation. This detail is commonly used according to the database of construction drawings gathered. A $400 \text{ mm} \times 400 \text{ mm}$ beam was built at the top of the wall and was used to apply the axial load with prestressing strands attached to the foundation beam at both sides of the wall. The top 1.7 m wall extension had a 1200 mm × 100 mm rectangular section and additional reinforcement to ensure the nonlinear behavior at the bottom wall. An initial axial load ratio (ALR) of 5% and 8% were applied to W1 and W2 respectively and the M/VL_w ratio was 3.75. These values were representative of the gathered database. The axial load was defined as the key variable as the database indicates that the height of the building inventory has gradually increased in time.

The walls were instrumented with eight (8) LVDT along both lateral edges (P1 to P8) (Fig. 2), one LVDT to capture sliding between the wall and the foundation beam and six (6) strain gauges (SG 1 to SG 6) to capture the strain of the reinforcing steel at the wall-foundation interface. One additional potentiometer (P9) was used to measure the out of plane displacement. This potentiometer was attached to an external fixed column and slid on the surface of the wall. The force load on the prestressing strands was allowed to vary during the tests as these were fix anchored at both ends, however, the strand forces were constantly measured with load cells (LC 1 and LC2). This load variation was allowed in an attempt to capture the effect induced by the coupling of the walls with the floor slab, which appears during an earthquake as the building deforms [24]. The wall was restrained in the out of plane direction by a 150 mm \times 150 mm rectangular steel tube that allowed the

Table 3Failure mode description for the wall database.

Author	Failure mode						
Oesterle et al. [21]	RW1 presented reinforced bar buckling followed by fracture. RW2 presented large out of plane displacements followed by fracture of some reinforcement bars and extensive concrete crushing. Yielding of boundary flexural reinforcement occurred at approximately 0.75% lateral drift, and vertical splitting and minor crushing of concrete at the wall edge were observed for 1% lateral drift. Failure was reached due to the buckling of the steel reinforcement bar in						
Thomsen and Wallace [22]							
Su and Wong [23]	compression and fracture of the steel in tension. Limited drift ratios as low as 1.1% were obtained and the effect on drift capacity from doubling the transverse reinforcement area is negligible for significantly high axial load ratios (ALR = 0.50). Failure of the walls						
Alarcón et al. [24]	exhibited out-of-plane behavior with an inclined surface after concrete crushing. Failure modes were characterized by vertical cracks at the wall ends followed by concrete crushing, reinforcement bar buckling and out-of-plane						
Hube et al. [20]	displacements. As ALR increased (ALR = 0.15 to 0.35), failure occurred more rapidly after concrete spalling. The results obtained provided evidence of behavior improvement (strength, ductility factor and dissipate energy capacity) as the transverse steel spacing (s/db = 9.0 in wall 1 to 4.5 in wall 8) is reduced and the						
	transverse steel ratio (0.44% in wall 1 to 0.64% in wall 8) and number of confinement legs increase. The behavior of the tested walls was relatively ductile. There was a significant variation on the drift ratio capacity, from 1.6% to 2.7%, depending on the transverse reinforcement detailing. There was a reduction in the drift capacity with the reduction of shear span as well as with the reduction of the wall thickness. The observed failure mode of the six tested walls was the out-of-plane wall buckling after the						
Pilakoutas and Elnashai [25]	compressive failure of the wall base. The maximum strength and deformation were not significantly affected by the variation in shear reinforcement. The plastic deformation took place within						
Goodsir [26]	the lower quarter of the wall. The most common failure mode was local concrete crushing followed by a kinking of the wall due to bar buckling which produced a permanent out-of-plane displacement. Vertical cracking at the wall edges and inclined transverse failure surface were also observed.						
McMenamin [27]	Failure was reported as an asymmetric crushing and spalling of the cover concrete, local reinforcement buckling and inclined transverse plane failure. W4, with a lighter steel ratio, presented fracturing of the reinforcement bars in tension and negligible out-of-plane deformation. Vertical cracks were observed at the wall edges, and plastic hinge length concentrated at the wall base was a characteristic for both specimens. The author also discussed the unlikelihood of obtaining lateral buckling failure mode due to the large out-of-plane shear						
Chiewanichakom [28]	stresses that cause an inclined transverse failure surface Out-of-plane deformation and twisting of the wall along its longitudinal axis were observed and explained as an effect from the buckling of the bars. None of the walls presented out-of-plane failure in spite of the large out-of-plane deformation in some of the walls, and the failure was caused by either concrete crushing or fracture of reinforcement. Fracture of the reinforcement bar was associated with premature fatigue caused by buckling						
Almeida et al. [17]	during cyclic loading. These tests were included in the rectangular wall database as the steel reinforcement in the flanges is very light inducing just a minimum effect on the neutral axis depth of the web. TW1 had out of plane displacements larger than 50% the wall thickness and a maximum drift of 0.7% to failure.						

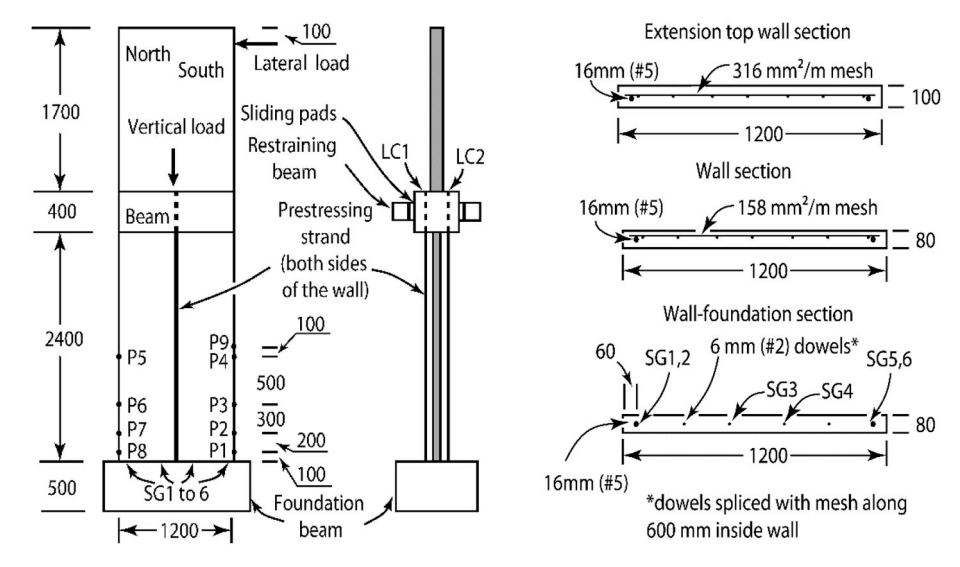


Fig. 2. Specimen details and instrumentation (units in mm).

in-plane movement of the wall due to sliding pads located between the concrete and the steel.

The wall was cast horizontally and then placed vertically in the reaction frame using a reinforced framework to prevent cracking or damage during the installation process. The concrete had an unconfined compression strength of 21 MPa. The 16 mm (#5) reinforcing bars had a 454 MPa yield strength, a 646 MPa ultimate strength and an 11.5% ultimate strain. The 5.5 mm wires from the electro-welded mesh had a 675 MPa yield strength and a 750 MPa rupture strength with a rupture strain of 2.5%. The steel for the 6 mm (#2) dowels connecting the wall to the foundation reached 520 MPa at yield and a rupture strength of 650 MPa for rupture strain of 4.5%.

A cyclic lateral force was applied to the walls following a load protocol as shown in Fig. 3, according to recommendations from Mergos and Beyer [29], which consider the cumulative damage effect for structures built in moderate or low seismic regions. This approach was selected because the tested walls represent elements used in moderate seismic regions and traditional loading protocols have been developed for high seismic regions, which may result in decreased strength and displacement capacities. Load protocol for the second test was adjusted based on results from the first test (see Fig. 3b).

5. Test results

5.1. Behavior and failure mechanism

A crack at the wall foundation interface with a maximum width of 0.15 mm appeared during the first load step of the 0.2% drift cycle and continued propagating horizontally during the same drift cycles, for both walls. In subsequent cycles (drift ratios equal to 0.35% and higher), several inclined cracks with low angle were observed at the middle of the wall cross section and spread approximately 600 mm in height from the foundation. There were some minor horizontal cracks spreading along the rest of the wall height which became more evident after cycle 5, corresponding to a lateral drift of 0.35%. During this cycle, the crack at the base of each wall opened up to an approximate size of 0.9 mm.

For W1 the same crack at the base opened up to 2 mm for the 0.5% drift cycle, and existing cracks along the wall had a maximum width of 0.55 mm. For the 0.75% drift cycle, the same specimen presented a slight out-of-plane displacement of 2 mm, and cracks spread along the length of the wall. W2 presented the first cracks along the height of the wall during the 0.4% drift cycle, and at 1% drift the foundation-wall interface crack opened up to 2 mm while the maximum crack width along its height was 0.4 mm. The wall-foundation crack width gradually increased for both specimens until the concrete spalled in a section that reached approximately 400 mm high at the compression edge. The cracking pattern at the end of the test shows extended horizontal cracks.

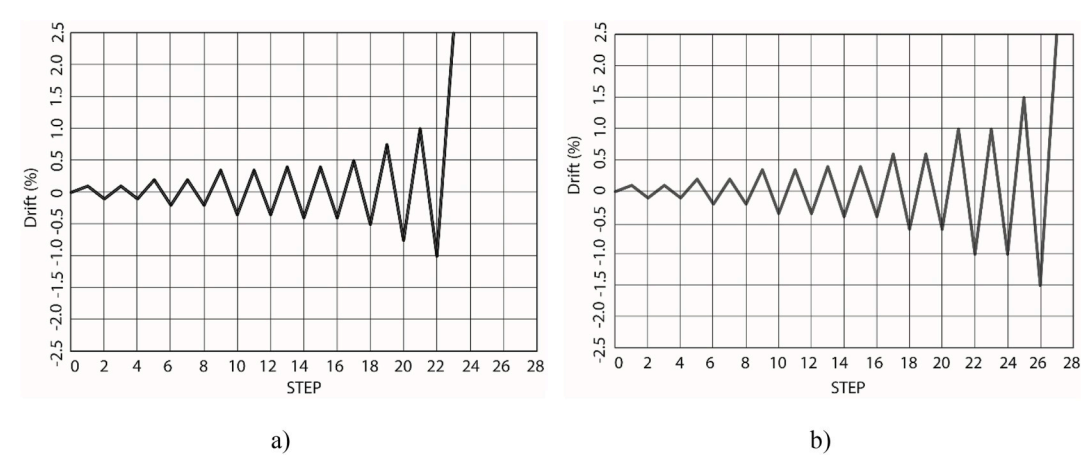


Fig. 3. Loading protocol a) W1 and b) W2.

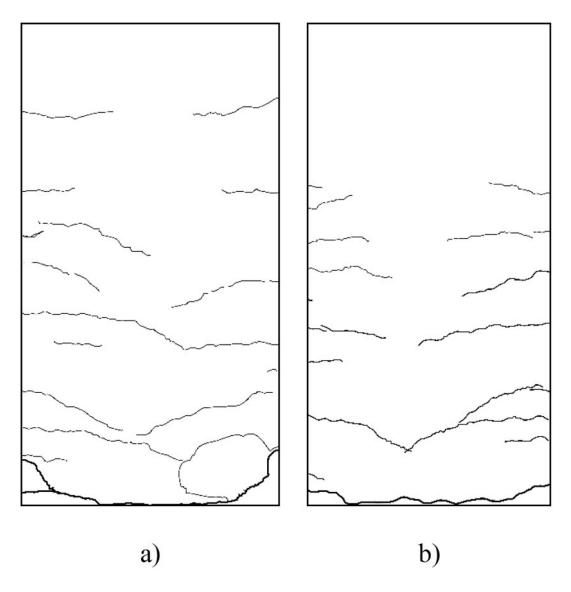


Fig. 4. Cracking pattern before concrete spalling at the wall toe. a) W1. b) W2.

slightly inclined at the bottom of the wall, with a larger concentrated crack at the wall-foundation interface (see Fig. 4). This large crack seem to be associated with a low reinforcement steel ratio as reported by Dazio et al. [10].

Both walls had similar failure patterns that consisted of concrete spalling at both wall edges and buckling of the reinforcing bar in the out-of-plane direction of the wall, at the compressed side during the last load step (see Fig. 5a and Fig. 6b). The buckled length was similar for both tests and was close to 150 mm, which coincides with the spacing of the wires of the electro-welded mesh, which seems to indicate that the mesh may have a restraining effect on the lateral displacement of the reinforcement bar until the concrete spalls.

The damage at the bottom of the walls also seem to indicate a concrete splitting contribution to the failure as vertical cracks propagated upwards, approximately 350 mm from the foundation, along the 80 mm side of the wall. For W1, this vertical crack resulted in the splitting of a 350 mm height by 100 mm long and 80 mm width concrete section at the side under tension during the last loading step, leaving the steel reinforcement bar completely exposed (see Fig. 5b). It was also evident that this crack resulted in the spalling of the concrete at the compressive side during the last load step, allowing the reinforcement to buckle in compression. (see Fig. 6b). Both specimens showed a large residual horizontal crack at the foundation-wall interface indicating that plastic rotation concentrated at this location (see Fig. 6a).

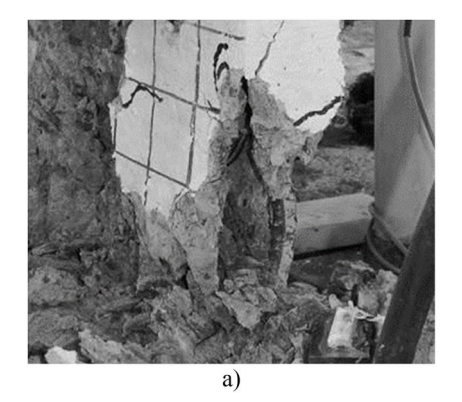




Fig. 5. W1 failure details ($50 \text{ mm} \times 50 \text{ mm}$ grid). a) Side under compression during last load step. b) Side under tension during the last load step.

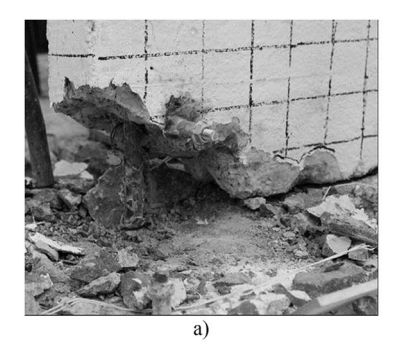




Fig. 6. W2 failure details ($50 \text{ mm} \times 50 \text{ mm}$ grid). a) Side under compression during last load step. b) Side under tension during the last load step.

5.2. Hysteretic behavior

The hysteretic response of the walls presented relatively narrow and stable cycles with a marked post yield slope (Fig. 7). Due to a malfunction of the data acquisition system for the W1 test, the data recorded was unreliable for loads larger than 34 kN in the pull direction. However, the data that was captured in this direction for previous cycles was similar to the data in the push direction and the hysteretic response in the missing portion was inferred, assuming symmetric responses in both directions, which was the case for W2. With the lowest axial load ratio, specimen W1 reached a maximum lateral load of 59.3 kN for an ALR of 8% and 1.0% drift, followed by a strength degradation until failure at 2.3% drift. Failure was defined at 80% of the maximum lateral force. Specimen W2, on the other hand, reached a slightly larger load capacity of 68.2 kN at 2.1% drift, when the ALR was approximately 15%, rapidly followed by failure at a drift of 2.2%. Axial load ratio variation in the direction of failure for W1 started from 5% and increased to 9.3% while for W2 the ALR started at 8% and doubled to 15.9% before failure (Fig. 8).

A local effect at the wall toe subjected to compression seems to have caused a strength drop for W1 at a lower drift than for W2. The vertical crack located at the wall toe compression was observed earlier for W1 than for W2 at a drift that corresponded approximately to the instant where strength drop started. There is an evident effect of the axial load increase on the lateral strength of the walls, in particular for W2, which had the largest ALR increase.

6. Discussion

The main concerns about the thin walls under study are the applicability of existing design conditions such as effective stiffness, plastic hinge length and boundary element requirements to this particular type of element and the drift capacity of these thin walls. All of these are discussed in the following sections.

6.1. Stiffness degradation

The Secant Stiffness Ratio (SSR) was defined as the relation between secant stiffness (K_s) for each drift during the first loading cycle, and the initial stiffness (K_o), obtained from the maximum displacement and force measured during the first cycle. The relation between SSR and drift of specimens tested are plotted in Fig. 9. Both specimens exhibit the same tendency. The lateral stiffness showed a significant degradation as drift increased for both specimens, reaching a loss of stiffness between 63% and 72% just at 1% lateral drift. The limited cracking in the wall and the size of the cracks seem to indicate that the source of the stiffness reduction is mainly due to the damage and crack evolution at the wall-foundation interface.

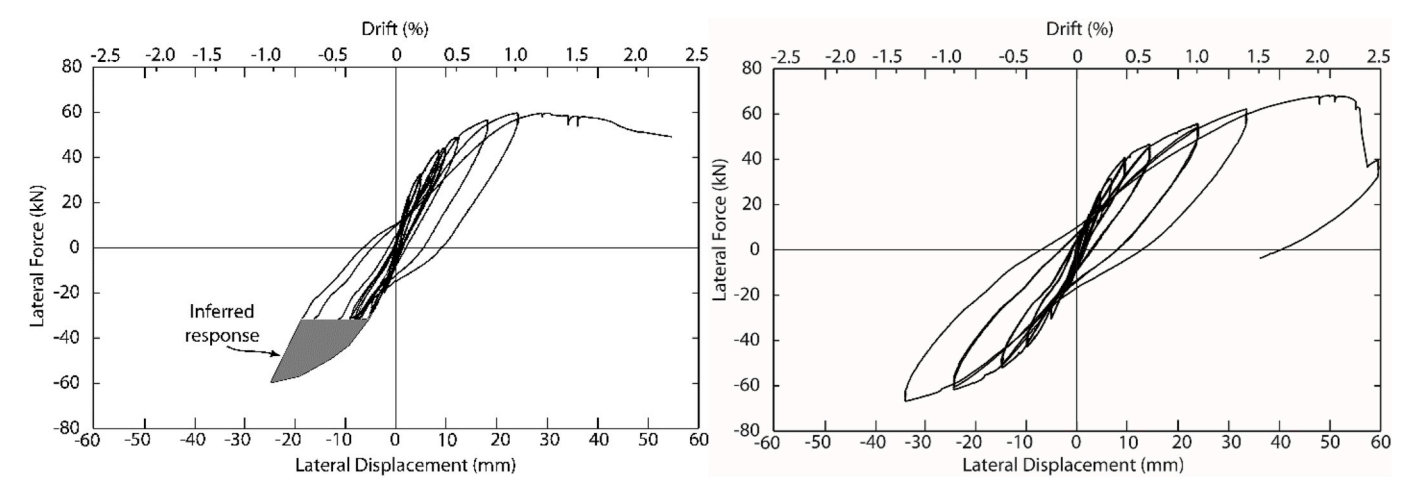


Fig. 7. Hysteretic response of wall - W1 (left) and W2 (right).

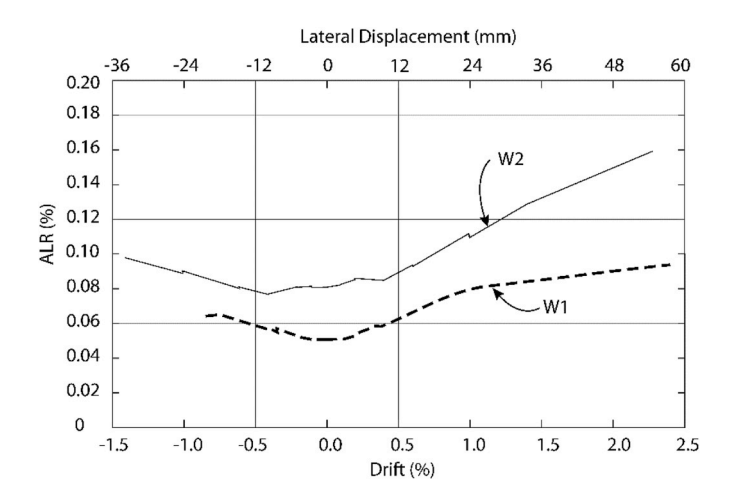


Fig. 8. Axial load variation.

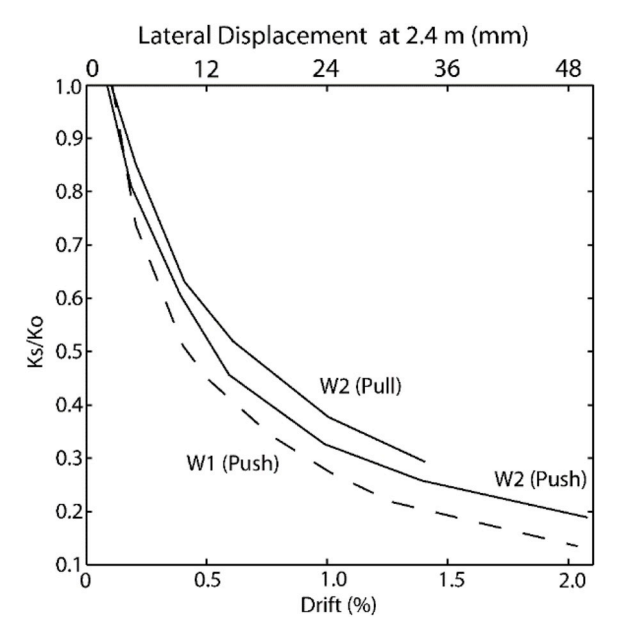


Fig. 9. Secant stiffness degradation ratio.

6.2. Plastic hinge length

The measurements from strain gages and linear potentiometers placed on W1 and W2 were used to estimate the curvature distribution for different load stages within the limits that the sensors captured useable readings. Maximum curvatures for both walls were located along the first 250 mm from the wall base, corresponding to 10% of the story height, which indicates a concentration of the plastic deformation in this region and a reduced plastic hinge length. This was evidenced by the crack distribution, where a large crack opened right at the foundation beam-wall interface. Fig. 10 shows the curvature distribution with respect to the normalized story height (2.4 m).

Plastic hinge length for walls have been reported to be close to half the element length and with a minimum length equal to the strain penetration of the steel at both sides from the yield location [15]. This minimum length can be estimated as a function of the yield strength (f_y) and the bar diameter (d_b) (see Eq. (1)). The plastic hinge length (l_p) of the tested walls was back calculated according to Eq. (1) and Eq. (2) based on the total wall height (H_w) , yield lateral displacement (Δ_y) , total lateral displacement (Δ_t) , and plastic curvatures (ϕ_p) measured from the test. The data was complemented with the test of specimen TW1, reported by Almeida et al. [17], which had close characteristics to W1 and W2. TW1 was 80 mm thick and had a single reinforcing mesh with an unconfined boundary element of 16 mm reinforcement bars and small diameter

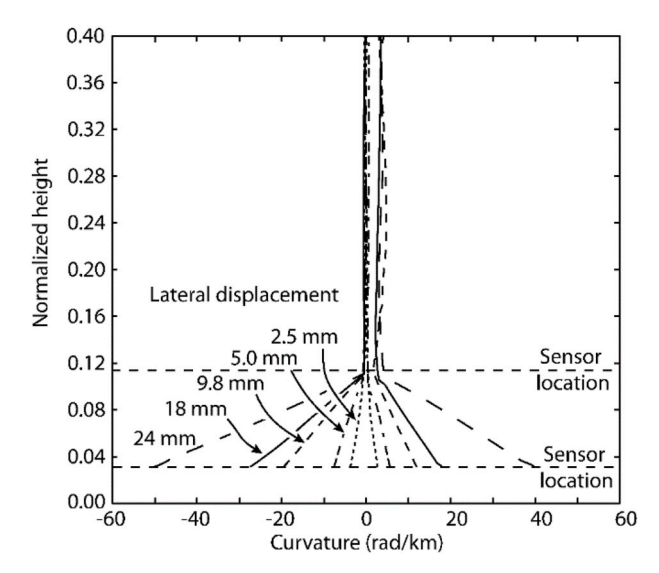


Fig. 10. Curvature distribution - W2 specimen.

reinforcement bars distributed along the wall length – $5.5\,\mathrm{mm}$ for W1 and W2 and 6 mm for TW1- with a similar steel ratio along the web as W1 and W2. The aspect ratio (M/L_wV) for TW1 was 3.7, while for W1 and W2 it was 3.5. The out-of-plane slenderness ratio was 25 for TW1 and 30 for W1 and W2.

$$L_p = 0.022 f_y d_b {1}$$

$$\Delta_t = \Delta_v + \phi_p L_p H_w \tag{2}$$

The progression of the plastic hinge length that could be captured by the sensors, as shown in Fig. 11, indicates that this length is significantly shorter than values currently defined by existing equations summarized elsewhere [30], which, assuming a nominal yield stress of 450 MPa, results in a value of 9.9 d_b. Back calculated results show a value between 6 d_h and 14 d_h for displacements close to failure, which indicates that the hinge is mainly controlled by the steel yield penetration. Rotation is concentrated along the wall-foundation interface, and cracking and nonlinear behavior of the wall above the interface is limited. Alarcón et al. [24] had already reported a short hinge length between 4 t_w to 5 t_w to match the experimental displacement obtained from their tests. However, the results from W1 and W2 from the tested walls resulted in a much shorter range between 1.2 t_w to 2.7 t_w which is closer to the value of 2.5 t_w proposed by Takahachi et al. [11]. The minimum value recommended by Hoult [31] of 100 mm results in L_p/d_b of 6.2, considering a bar diameter of 16 mm which was used at the edges for W1, W2 and TW1. This evidence indicate that for thin lightly reinforced walls, values as short as 6.0 d_b may be plausible for numerical analyses.

6.3. Boundary elements

According to the current local regulation in Colombia, based on ACI 318–08 [2], boundary elements in special reinforced concrete walls should be used following Eq. (3a), where c is the neutral axis depth and $\Delta_{\rm u}$ is the top lateral displacement of the wall. The most recent version of ACI-318 introduced a stricter condition as shown by Eq. (3b) [32] to limit the damage of the element. This equation however has been defined using displacement design principles, assuming a plastic hinge length equal to half the length of the wall $(L_p = L_w/2)$. This assumption however is not accurate according to the data shown in the previous section. Considering the limitation from the previous equations, Hoult et al. [33] proposed using a plastic hinge length of $L_p = 0.2L_w$, resulting in Eq. (3c).

$$c \ge \frac{L_w}{600 \left(\Delta_u/H_w\right)} \tag{3a}$$

$$c \ge \frac{L_w}{600\left(1.5\,\Delta_u/H_w\right)}\tag{3b}$$

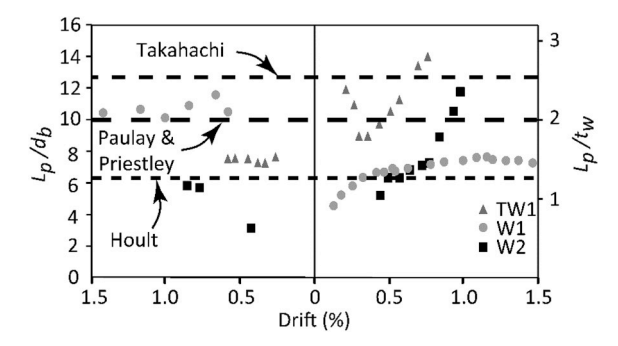


Fig. 11. Plastic hinge progression.

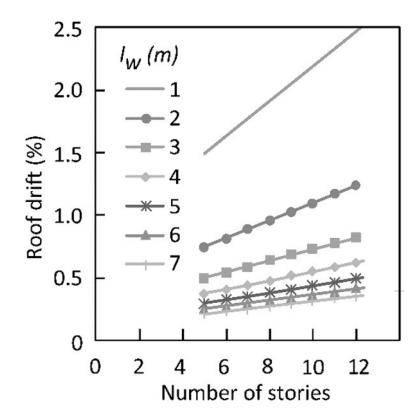


Fig. 12. Roof drift ratio at maximum concrete strain.

$$c \ge \frac{L_w}{1500\left(1.5\,\Delta_{u/H_w}\right)}\tag{3c}$$

The same displacement design principles applied for Eq. (3) were used to obtain the maximum roof drift ratio of unconfined walls with different lengths and buildings with different number of stories (Fig. 12) according to Eq. (4). This equation was obtained considering the elastic and plastic displacements, where the former was estimated considering a previous work by Massone and Alfaro [34]. The latter was estimated considering a plastic hinge length of 3 times the wall thickness (t_w), an ultimate concrete strain of 0.003 and a neutral axis depth of 0.1 L_w . This value is considered approximately accurate for walls with an axial load ratio close to 5% [35]. Note that the considerations applied to obtain Eq. (4), specifically the short plastic hinge and the limited elastic displacement, result in significantly smaller drift ratios values than those expected from commonly used equations where the elastic displacement (\varDelta_y) can be as large as $\varDelta_y = 0.67 \frac{\epsilon_y}{L_w} H_w^2.$ This expression is three times larger than the proposal by Massone and Alfaro. Additionally, the plastic hinge length, as previously discussed, is commonly estimated as $L_p =$ $L_w/2$, which can be also several times larger than the 3 t_w presented by Takahashi et al. [11]. The equation is hereby presented to analyze the effect of the wall length, however, it validity is to be confirmed by more detailed analyses of complete building models.

$$\frac{\Delta_t}{H_w} = 0.22 \frac{\varepsilon_y}{L_w} H_w + \left(\frac{\varepsilon_{cu}}{c} - 1.4 \frac{\varepsilon_y}{L_w}\right) *3t_w \tag{4}$$

As expected by section analysis and displacement design principles,

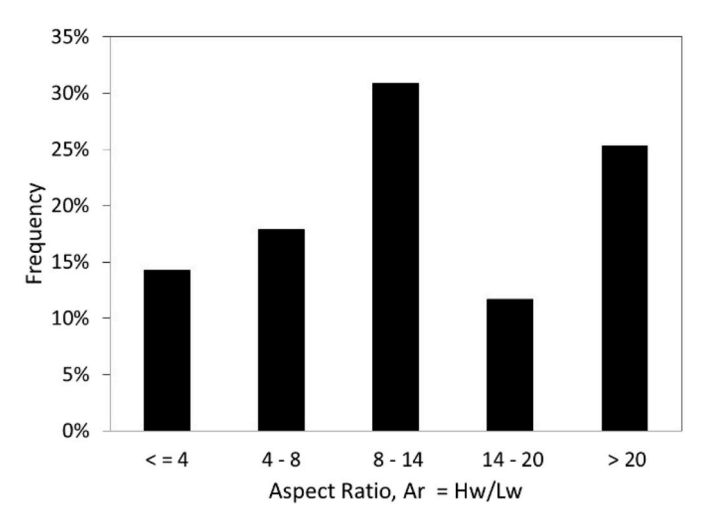


Fig. 13. Distribution of aspect ratio, Ar.

longer walls have shorter displacement capacity, and considering that, the evaluated building database indicates that the controlling wall length may be between 4 m to 6 m, design drifts should be kept relatively low. The distribution of the aspect ratios of the building in the database (Fig. 13) indicate that approximately 35% of the walls have an aspect ratio below 8, and are the ones that will have nonlinear demands on the building.

6.4. Out-of-plane slenderness ratio

The lateral drift capacity of the tested walls W1 and W2 was complemented with results from the twenty-eight specimens from the experimental database previously discussed, and the results from the tests reported herein are shown in Fig. 14 and classified according to ALR, number of reinforcing layers, and confinement or no confinement. Drift ratios are plotted against the ratio of story clear height to wall thickness (H_w/t_w) , given that the latter variable has been identified as a key design parameter to prevent out-of-plane instability [36]. An H_w/t_w value of 16 is included in the same figure because it is currently defined as the out-of-plane slender ratio limit in the compression zone for special structural walls by ACI 318-14 [32]. The ALR was divided into three ranges based on the analyses of the building database as follows: most of the walls in the buildings evaluated present an ALR below 10%. Few walls presented ALRs larger than 0.10 but, under gravity loads, ALRs larger than 0.18 were not identified. Coupling of walls due to slab kinematic interaction under lateral loads will increase the axial loads in the walls; however, this effect was not evaluated for the building inventory.

Tested walls (W1 and W2) reached drift ratios larger than 2% even with the out-of-plane slenderness ratio of 30. The drift capacity for these specimens is comparable to specimens with a larger thickness and with better confinement detailing than those tested by Goodsir [26], which had similar out-of-plane slenderness ratios. Similar drift ratios were obtained by Thomsen IV and Wallace [22] and Hube et al. [20], for specimen with larger out-of-plane slenderness ratios and better confinement detailing. It is important to note that there is an significant difference among the load protocol applied to these tests. As previously

mentioned W1 and W2 were subjected to a protocol with a reduced number of large cycles, with the intention of limiting the energy introduced to the walls and obtaining information that could be related to moderate seismic zones. The experimental evidence is still scare, however it is likely that performance was improved simply by limiting the number of large cycles so reinforcement bar buckling would occur at larger drift values.

Drift capacities above 1.5%, which could be an expected maximum demand drift limit [37], were obtained for all the specimens except for two of the walls with a high axial load level, for walls with out-of-plane slenderness ratio larger than 50 and for the particular case of TW1, which was the longest specimen included in the experimental database. These results confirm the expected impact in the reduction of the drift capacity with the increase of the axial load, the wall length and the out-of-plane slenderness. The reduction pattern of the drift capacity can also be observed as a function of the wall length (L_w) to wall thickness (t_w) normalized ratio (Fig. 15).

It is important to mention that the experimental data comes from specimens with a length less than 1.5 m with the exception of TW1, which is 2.7 m long. As previously mentioned, walls between 4 m and

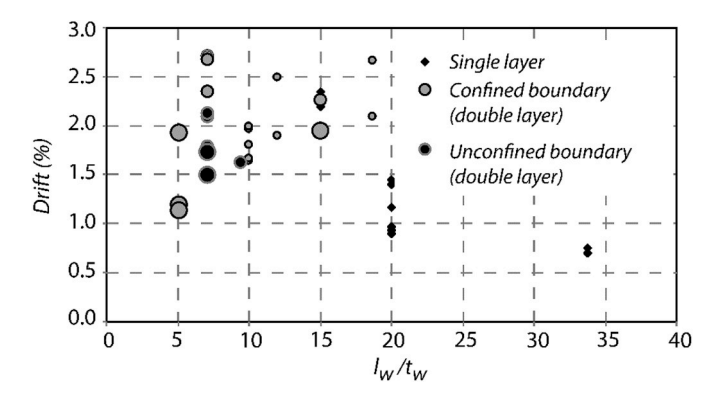


Fig. 15. Wall length effect on maximum drift from experimental database.

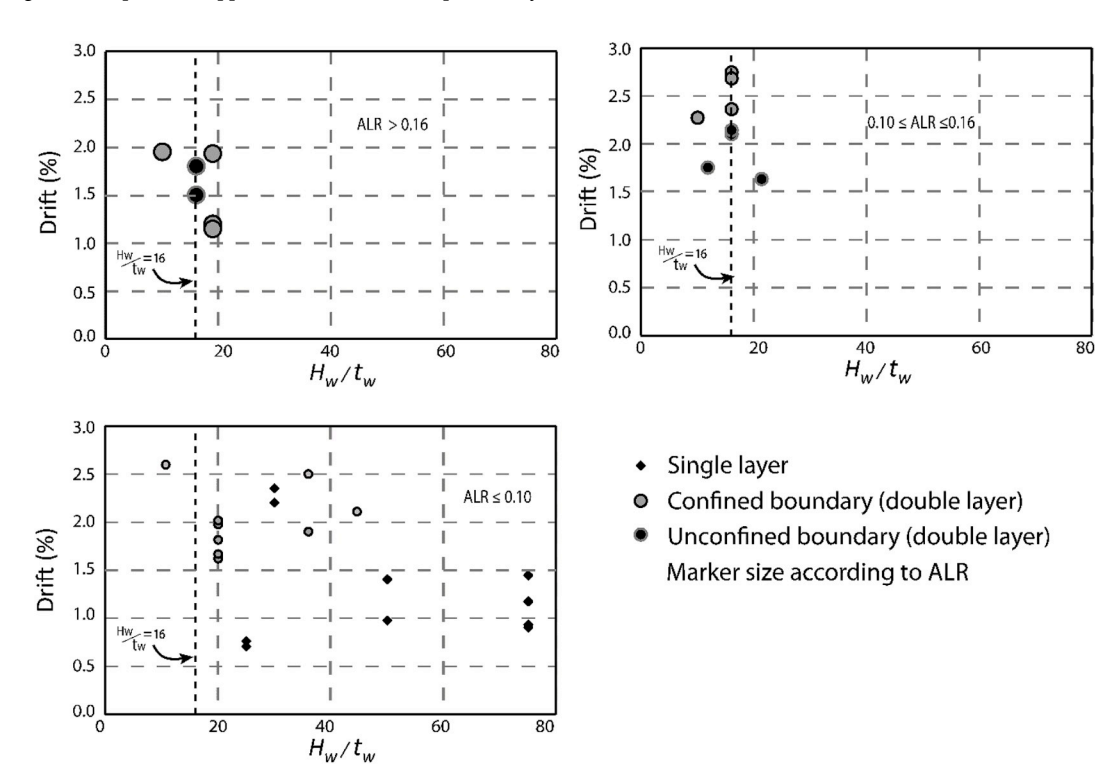


Fig. 14. ALR effect on maximum drift from experimental database.

6 m are common in the buildings evaluated and it would not be accurate to extrapolate directly the experimental drift capacity from the tests to the most representative walls in the buildings. However, it is clear that the trends indicate as the wall length and out-of-plane slenderness increases, the drift capacity is reduced. Axial load is also of importance, but for the long walls in the buildings from the database, the ALR is very low (<5%). Another observation from the experimental database is that short walls, with a single reinforcement layer, no confined boundaries and low thickness as W1 and W2, may accommodate drifts larger than 1.5%. These walls could be used if there are other well-detailed walls to provide most of the lateral resistance of the structure.

6.5. Capacity-demand analyses

The experimental database shows that the drift capacity of rectangular walls may be limited, especially when there is no boundary elements, the thickness is reduced or the wall length increases. To evaluate this limited drift capacity at global structural level, a total of 35000 nonlinear analyses of probabilistically defined single degree of freedom simplified models, representative of building archetypes of 6, 7, 8, 9 and 10 stories (see Fig. 16), were carried out. Buildings above 10 stories were not included as, based on the gathered database, structural detailing and thickness of the walls for taller buildings may have significant differences.

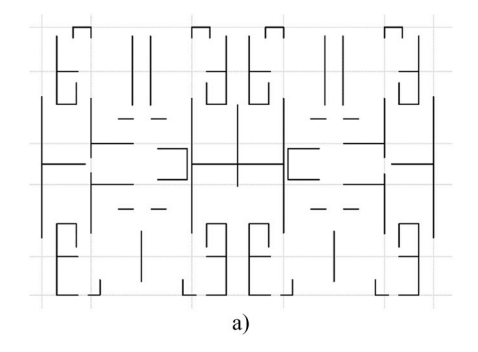
The models were defined based on 14 buildings from the database, which were located in a moderate seismic region. Based on the building database, probability distribution functions were obtained for some of the main variables that control the seismic behavior, such as the aspect ratio, wall area, axial load ratio and compression concrete strength. For each archetype, one hundred structural models were generated to represent different types of structural configurations. Each model was defined considering rectangular walls with different aspect ratio: Long walls $(2 \le Ar < 6)$, intermediate walls $(6 \le Ar < 10)$ and short walls (Ar > 10). The models were considered to have rectangular walls only and a web reinforcement ratio of 0.0025 in the longitudinal and transverse direction. The wall thickness was set to 100 mm with a single curtain of reinforcement, which usually consists of cold-drawn welded wire mesh. This reinforcement is the minimum required according to the current local regulation of the buildings in the database. To meet the ultimate flexural demand, additional ductile reinforcement bars were considered at the edges of the walls. The number of walls for each model was defined based on the base shear obtained from empirical fundamental period of the model and the design spectrum of the Colombian code for a C-type soil (shear wave velocity between 760 m/s and 360 m/ s), an intermediate seismic hazard zone (PGA = 0.15 g). The shear for each wall was distributed proportional to the square of its length. A detailed description of the methodology is presented in Bonett et al. [38].

The structural models were defined as equivalent Single-Degree-Of-Freedom (SDOF) oscillators. Each SDOF was defined in terms of effective modal masses, effective stiffness, fundamental period and the modal

participation factors of the first mode of vibration. For each one of the one hundred models, for each archetype, capacity curves were obtained from nonlinear incremental static analyses and the maximum roof drift ratio capacity (RDR) was calculated. The maximum capacity of the walls was defined for a severe damage limit state where the extreme fiber compression strain reaches 0.003 or one of the steel dowels connecting the wall and the foundation reaches the fracture strain ($\varepsilon_{su} = 0.045$) [4]. Welded wire mesh has a more limited fracture strain ($\varepsilon_{su} = 0.0095$) [39], however, as the plasticity is concentrated at the wall-foundation interface, the ultimate strain for the analyses correspond to the steel with the lowest strain capacity placed at this location. The seismic demand at the base of the models was represented by 70 ground motion records, which were selected from the PEER (Pacific Earthquake Engineering Research) database. These records are representative of the tectonic environment and seismicity of South America according to the analyses reported by Villar-Vega et al. [40]. The selected set consist in the ground motion records with values of PGA between 0.25 g and 2.3 g. The records were scaled considering a maximum scaling factor of 5. The levels of intensity were defined between 0.2 g and 2.0 g. Considering the range of number of stories (6 to 10), the records were increasingly scaled to macth a predefined spectral intensity between these acceleration limits for a structural period of 0.3 s. The maximum roof drift ratio demand for each model was calculated by means of nonlinear time history analysis (NLTHA) of SDOF systems using the GEM's Risk Modeller's Toolkit [41]. This module relies on the open-source software for nonlinear structural analysis OpenSees [42] to perform the NLTHA on the SDOF systems. The hysteresis model of each SDOF was defined using the "Pinching4 Material" model [43] with structural degradation in both stiffness and strength, calibrated from the experimental results. The nonlinear dynamic analyses were performed with the standard pinching parameters from OpenSees. A statistical analysis of the RDR capacity and demand based on a box-and-whisker chart was carried out to assess statistically data results for each building (Fig. 17). In general terms, it is observed that the capacity is always greater than the demand, except for the 10-story archetype, where in some cases, the roof drift ratio demand could exceed the roof drift ratio capacity. Therefore, the evaluated archetypes have a low likelihood of reaching a severe damage limit state.

7. Conclusions

This paper analyzes the experimental behavior of thin slender rectangular concrete reinforced walls with characteristics that are representative of a typology of buildings used in some Latin American countries in moderate seismic zones. Results from an experimental program are complemented with existing results, which, although they do not exactly adjust to the typology evaluated, present key characteristics that provide insight into the behavior of the thin slender walls studied. The experimental database indicate that as the axial load, wall length and wall out-of-plane slenderness increases the drift capacity can be reduced reaching values as low as 0.7%. The same database and the walls tested as part of the study also show that short length walls,



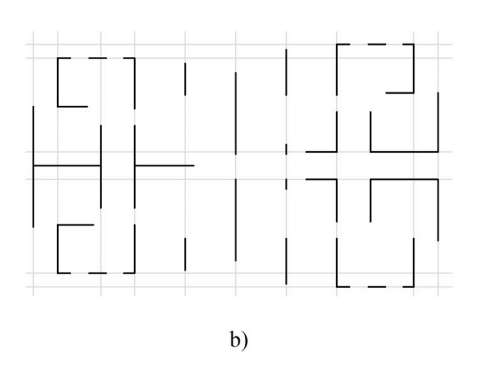
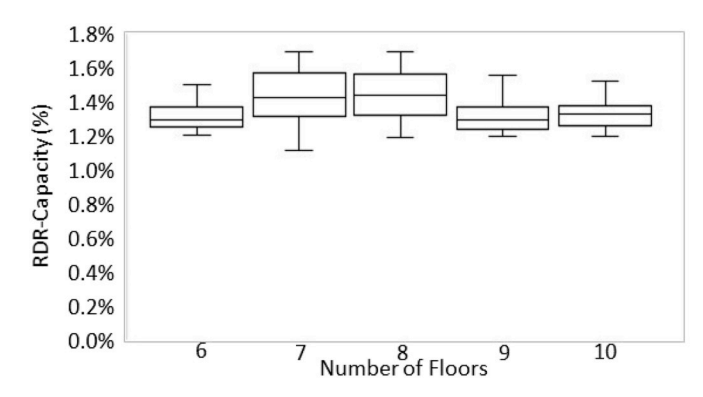


Fig. 16. Typical floor plans for the archetypes. a) $18 \text{ m} \times 23 \text{ m}$ building b) $12 \text{ m} \times 19 \text{ m}$ building.



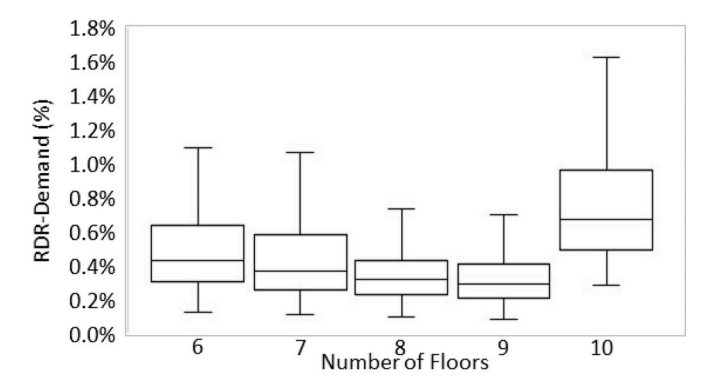


Fig. 17. a) RDR capacity and b) RDR Demand of 6-to 10 story buildings.

exceeding the ACI recommended out-of-plane slenderness limit (H_W/T_W) of 16, may reach drift limits in excess of 1.5%; however, these do not control the seismic building performance. The results for these short walls are relevant however to indicate that, if there are well detailed long walls in the structure, short walls with a single steel layer and no confined boundaries may be used for these buildings. Additionally, it would not be necessary for these short walls to have the same thickness of long walls requiring confinement for preventing concrete crushing and reinforcement localized buckling.

The walls tested in this study showed drift capacities above 2% in spite of the thickness and reinforcement characteristics. The experimental data is still scarse, but this behavior could be attributed to the load protocol applied, which was adjusted for walls located in moderate seismic regions. Further testing of longer walls with similar load protocols could be useful to verify this hypothesis.

Tests also revealed that typical plastic hinge length equations are not adequate for the wall typology evaluated because the plasticity is concentrated at the wall foundation interface and has a limited spread along the wall height. Maximum calculated values for plastic hinge length result in approximately $15\ d_b$ or $3.0\ t_w$ but these could be as low as $6.2\ d_b$ or $1.2\ t_w$. These hinge values also result in that current ACI equations, for defining the use of boundary elements, do not manage to provide reliable results for the wall typology evaluated. Therefore plastic hinge lengths as low as the steel strain penetration should be considered to apply formulations based on displacements or to verify material strains at the wall base.

In spite of the limited drift capacity of the walls, typical structural configurations of buildings with thin slender walls from six to ten stories, have low displacement demands in moderate seismic regions. The wall area ratios seem to result in rigid buildings with an average roof drift ratios capacity which is 80% larger than the roof ratio demand for the worst case evaluated, corresponding to the ten story height building. The probabilistic dispersion of the results show that the severe damage probability is low for the same case. It is important to consider however that the analyses were carried out idealizing the structure with rectangular wall elements only. Non-rectangular walls have a different behavior to rectangular walls, which should be further studied. Results are also applicable for the expected hazard level and the soil profile analyzed.

Declaration of competing interest

The authors of the manuscript "THIN SLENDER CONCRETE RECT-ANGULAR WALLS IN MODERATE SEISMIC REGIONS WITH SINGLE REINFORCEMENT LAYER" certify that they have NO affiliations with or involvement in any organization or entity with any financial interest (such as honoraria; educational grants; participation in speakers' bureaus membership, employment, consultancies, stock ownership, or other equity interest; and expert testimony or patent-licensing arrangements), or non-financial interest (such as personal or professional

relationships, affiliations, knowledge or beliefs) in the subject matter or materials discussed in this manuscript.

Acknowledgements

This work was supported by Universidad EIA, Universidad de Medellin (Colombia) and the following Colombian companies and associations: CAMACOL Regional Antioquia, Doing Estudios de Ingeniería, Industrias del Hierro and CONCONCRETO. The authors gratefully acknowledge the assistance of Jose Fernando Rave and the undergraduate students of the Civil Engineering Departments of Universidad EIA and Universidad de Medellin with the experimental test. We thank Professor Katrin Beyer and Dr. Joao Almeida at the Earthquake Engineering and Structural Dynamics Laboratory of the École Polytechnique Fédérale de Lausanne (EPFL) for working with us during the experimental stage and providing the TW1 data. The funds provided by EPFL's Cooperation & Development Center (CODEV) for the TW1 tests are also greatly appreciated. This work was carried out as part of the initiative towards seismic risk reduction of the Colombian Earthquake Engineering Research Network (CEER).

References

- AIS, Reglamento Colombiano de Construcción Sismo. "Resistente NSR-10.", Asociación Colombiana de Ingeniería Sísmica, Bogotá, Colombia, 2010.
- [2] American Concrete Institute (ACI), Building Code Requirements for Structural Concrete and Commentary, 318, ACI, 2008, 08.
- [3] C.A. Arteta, J. Sánchez, R. Daza, C. Pájaro, C.A. Blandón, R.L. Bonett, J. Carrillo, Thin Wall Reinforced Concrete Building Database for the City of Armenia (Colombia) and Testing Specimen Selection. Report 001 CEER – Colombian Earthquake Engineering Research Center, 2016 (Barranquilla).
- [4] C.A. Arteta, C.A. Blandon, R. Bonett, J. Carrillo, Study about the Seismic Behavior of Thin Reinforced Concrete Wall Buildings: Report for Sub Committee C - AIS 100. Report 001 CEER – Colombian Earthquake Engineering Research Center, 2018 (Barranquilla).
- [5] R. Jünemann, M. Hube, J.C. De la Llera, E. Kausel, Characteristics of reinforced concrete shear wall buildings damaged during 2010 Chile earthquake, in: Proceedings of 15th World Conference on Earthquake Engineering, Portugal, Lisbon, 2012, 2012, Paper N2265.
- [6] Sri Sritharan, Katrin Beyer, Richard S. Henry, Y.H. Chai, Mervyn Kowalsky, Desmond Bull, Understanding poor seismic performance of concrete walls and design implications, Earthq. Spectra 30 (1) (2014) 307–334, 2014.
- [7] C. Alarcon, M.A. Hube, R. Junemann, J.C. De la Llera, Characteristics and displacement capacity of reinforced concrete walls in damaged buildings during 2010 Chile earthquake, Bull. Earthq. Eng. 13 (4) (2015) 1119–1139, https://doi. org/10.1007/s10518-015-9727-0.
- [8] W.Y. Kam, S. Pampanin, K. Elwood, Seismic performance of reinforced concrete buildings in the 22 February Christchurch (Lyttelton) earthquake, Bull. N. Z. Soc. Earthq. Eng. 44 (4) (2011) 239–278.
- [9] J.H. Thomsen IV, J.W. Wallace, Displacement-based Design of Reinforced Concrete Structural Walls: an Experimental Investigation of Walls with Rectangular and T-Shaped Cross Sections. Report No. CU/CEE-95-06, Department of civil and Environmental Engineering. Clarkson University, 1995. June 1995.
- [10] A. Dazio, K. Beyer, H. Bachmann, Quasi-static cyclic tests and plastic hinge analysis of RC structural walls, Eng. Struct. 31 (7) (2009) 1556–1571.
- [11] S. Takahashi, K. Yoshida, T. Ichinose, Y. Sanada, K. Matsumoto, H. Fukuyama, H. Suwada, Flexural drift capacity of reinforced concrete wall with limited confinement, ACI Struct. J. 110 (1) (2013) 95–104.

- [12] H. Dai, An Investigation of Ductile Design of Slender Concrete Structural Walls, MS Thesis, Iowa State University, Ames. IA, 2012, p. 134.
- [13] I.D. Lefas, M.D. Kotsovos, N.N. Ambraseys, Behavior of reinforced concrete structural walls: strength, deformation characteristics, and failure mechanism, Struct. J. 87 (1) (1990) 23–31.
- [14] Y. Lu, R.J. Gultom, Q.Q. Ma, R.S. Henry, Experimental validation of minimum vertical reinforcement requirements for ductile concrete walls, ACI Struct. J. 115 (4) (2018) 1115–1130.
- [15] T. Paulay, M.J.N. Priestley, Seismic Design of Reinforced Concrete and Masonry Buildings, Wiley, New York, 1992.
- [16] A. Rosso, L.A. Jiménez-Roa, J.P. de Almeida, A.P.G. Zuniga, C.A. Blandón, R. L. Bonett, K. Beyer, Cyclic tensile-compressive tests on thin concrete boundary elements with a single layer of reinforcement prone to out-of-plane instability, Bull. Earthq. Eng. 16 (2) (2018) 859–887.
- [17] J. Almeida, O. Prodan, A. Rosso, K. Beyer, Tests on thin reinforced concrete walls subjected to in-plane and out-of-plane cyclic loading, Earthq. Spectra 33 (1) (2017) 323–345. February 2017.
- [18] L.G. Quiroz, Y. Maruyama, C. Zavala, Cyclic behavior of thin RC Peruvian shear walls: full-scale experimental investigation and numerical simulation, Eng. Struct. 52 (2013) 153–167.
- [19] J. Carrillo, S.M. Alcocer, Seismic performance of concrete walls for housing subjected to shaking table excitations, Eng. Struct. 41 (2012) 98–107.
- [20] M.A. Hube, A. Marihuén, J.C. De la Llera, B. Stojadinovic, Seismic behavior of slender reinforced concrete walls, Eng. Struct. 80 (2014) 377–388, https://doi.org/ 10.1016/j.engstruct.2014.09.014.
- [21] R.G. Oesterle, A.E. Fiorato, L.S. Johal, J.E. Carpenter, H.G. Russell, W.G. Corley, Earthquake Resistant Structural Walls-Tests of Isolated Walls. Research and Development Construction Technology Laboratories, Portland Cement Association, 1976.
- [22] J.H. Thomsen IV, J.W. Wallace, Displacement-based design of slender reinforced concrete structural walls - experimental verification, J. Struct. Eng. 130 (4) (2004) 618–630, https://doi.org/10.1061/(ASCE)0733-9445(2004)130:4(618).
- [23] R.K.L. Su, S.M. Wong, Seismic behaviour of slender reinforced concrete shear walls under high axial load ratio, Eng. Struct. 29 (8) (2007) 1957–1965, https://doi.org/ 10.1016/j.engstruct.2006.10.020.
- [24] C. Alarcon, M.A. Hube, J.C. De la Llera, Effect of axial loads in the seismic behavior of reinforced concrete walls with unconfined wall boundaries, Eng. Struct. 73 (2014) 13–23, https://doi.org/10.1016/j.engstruct.2014.04.047.
- [25] K. Pilakoutas, A. Elnashai, Cyclic behavior of reinforced concrete cantilever walls, part I: experimental results, ACI Struct. J. 92 (3) (1995) 271–281.
- [26] W.J. Goodsir, The design of coupled frame-wall structures for seismic actions (Doctoral dissertation), http://ir.canterbury.ac.nz/handle/10092/7751, 1985.
- [27] A. McMenamin, The Performance of Slender Precast Reinforced Concrete Cantilever Walls with Roof Level Lateral Displacement Restraint under Simulated In-Plane Seismic Loading, Research Report 99-4, Department of Civil Engineering, University of Canterbury, Christchurch, New Zealand, 1999, 275pp.
- [28] Methee Chiewanichakorn, Stability of thin precast concrete wall panels subjected to gravity and seismic forces (Doctoral dissertation), Retrieved from, http://ir. canterbury.ac.nz/handle/10092/10450, 1999.
- [29] P.E. Mergos, K. Beyer, Loading protocols for European regions of low to moderate seismicity, Bull. Earthq. Eng. 12 (6) (2014) 2507–2530.
- [30] İ. Kazaz, An analytical study on the plastic hinge length of structural walls, ASCE. J. Struct. Eng. 139 (11) (2013) 1938–1950.
- [31] R. Hoult, H. Goldsworthy, E. Lumantarna, Plastic hinge analysis for lightly reinforced and unconfined concrete structural walls, Bull. Earthq. Eng. 16 (2018) 4825–4860, https://doi.org/10.1007/s10518-018-0369-x.
- [32] American Concrete Institute (ACI), Building Code Requirements for Structural Concrete and Commentary, 318, ACI, 2014, 14.

- [33] R. Hoult, H. Goldsworthy, E. Lumantarna, Seismic performance of lightly reinforced and unconfined C-shaped walls, in: Australian Earthquake Engineering Society 2017 Conference, 2017 (Canberra).
- [34] L.M. Massone, J.I. Alfaro, Displacement and curvature estimation for the design of reinforced concrete slender walls, Struct. Des. Tall Special Build. 25 (16) (2016) 823–841.
- [35] J.P. Moehle, T. Ghodsi, J.D. Hooper, D.C. Fields, R. Gedhada, Seismic Design of Cast-In-Place Concrete Special Structural Walls and Coupling Beams. NEHRP Seismic Design Technical Brief No, 6, 2011.
- [36] T. Paulay, M.J.N. Priestley, Stability of ductile structural walls, ACI Struct. J. 90 (4) (1993) 385–392.
- [37] J.W. Wallace, J.P. Moehle, Ductility and detailing requirements of bearing wall buildings, J. Struct. Eng. 118 (6) (1992) 1625–1644.
- [38] R. Bonett, J. Carrillo, C. Blandon, C. Arteta, J.F. Restrepo, J.L. Rosales, Evaluation of ductility reduction factors for thin and slender shear walls (in Spanish). IX Congreso Nacional de Ingeniería Sísmica. Mayo 29 a 31 de 2019. Santiago de Cali. Colombia, 2019.
- [39] J. Carrillo, C. Diaz, C.A. Arteta, Tensile mechanical properties of the electro-welded wire meshes available in Bogotá, Colombia, Constr. Build. Mater. 195 (2019) 352–362.
- [40] M. Villar-Vega, V. Silva, H. Crowley, C. Yepes, N. Tarque, A.B. Acevedo, M. A. Hube, C.D. Gustavo, H. Santa-María, Development of a Fragility Model for the Residential Building Stock in South America, Earthquake Spectra 33 (2) (2017) 581–604.
- [41] V. Silva, C. Casotto, A. Rao, M. Villar, H. Crowley, D. Vamvatsikos, OpenQuake Risk Modeller's Toolkit - User Guide. Global Earthquake Model. Technical Report 2015-09, 2015.
- [42] F. McKenna, G.L. Fenves, M.H. Scott, B. Jeremic, "Open System for Earthquake Engineering Simulation (OpenSees)," Pacific Earthquake Engineering Research Center, University of California, Berkeley, CA, 2000.
- [43] F. McKenna, M.H. Scott, G.L. Fenves, Nonlinear finite element analysis software architecture using object composition, J. Comput. Civ. Eng. 24 (2010).

Symbol list

- ϕ_p : Plastic curvature
- db: Steel reinforcing bar diameter
- f'c: Concrete compression strength
- f_{y}^{1} : Steel yield strength
- H_w : Wall specimen height
- K_s : Wall specimen secant stiffness
- Ko: Wall specimen initial stiffness
- L_b: Boundary element length
- L_p : Plastic hinge length
- L_w: Wall specimen length *M*: Overturning moment
- S: Transverse steel spacing
- tw: Wall thickness
- V: Shear force
- δ_{f} : Failure drift (%)
- Δ_u : Lateral displacement at ultimate limit state
- Δ_t : Total lateral displacement
- Δ_{ν} : Lateral yield displacement
- ρ : Total vertical reinforcement ratio
- ρ_h : Transverse reinforcement ratio